Synthesis and systematic optical investigation of selective area droplet epitaxy of InAs/InP quantum dots assisted by block copolymer lithography

Shikin, Artem; Lebedkina, Elizaveta; Ciostek, Czcibor; Holewa, Pawel; Ndoni, Sokol; Almdal, Kristoffer; Yvind, Kresten; Syperek, Marcin; Semenova, Elizaveta

Published in:
Optical Materials Express

Link to article, DOI:
10.1364/OME.9.001738

Publication date:
2019

Document Version
Publisher's PDF, also known as Version of record

Research Article Vol. 9, No. 4 / 1 April 2019 / Optical Material Express 1738
Optical Materials EXPRESS

Synthesis and systematic optical investigation of selective area droplet epitaxy of InAs/InP quantum dots assisted by block copolymer lithography

ARTEM SHIKIN,[1] ELIZAVETA LEBEDKINA,[1] CZCIBOR CIOSTEK,[2] PAWEŁ HOLEWA,[2] SOKOL NDONI,[3,4] KRISTOFFER ALMDAL,[3,4] KRESTEN YVIND,[1] MARCIN SYPEREK,[2] AND ELIZAVETA SEMENOVA[1,*]

[1]*DTU Fotonik, Technical University of Denmark, Kongens Lyngby DK-2800, Denmark*
[2]*Wroclaw University of Science and Technology, Faculty of Fundamental Problems of Technology, Laboratory for Optical Spectroscopy of Nanostructures Wroclaw 50-370, Poland*
[3]*DTU Nanotech, Technical University of Denmark, Kongens Lyngby DK-2800, Denmark*
[4]*DNRF Center for Nanostructured Graphene, Kongens Lyngby DK-2800, Denmark*
[*]*esem@fotonik.dtu.dk*

Abstract: We report on the synthesis and systematic investigation of quantum dot based optical gain material potentially suitable for applications in active devices operating around a wavelength of 1.55 µm and above. The quantum dots were selectively grown in a process assisted by block-copolymer lithography. We applied a new type of diblock copolymer, PS-b-PDMS (polystyrene-block-polydimethylsiloxane), which allows for the direct fabrication of a silicon oxycarbide hard mask used for lithography. Arrays of InAs/InP quantum dots were selectively grown via droplet epitaxy. Our detailed optical investigations of the quantum dot carrier dynamics in the 10-300 K temperature range indicate the presence of a significant density of defect states located within the InP bandgap and in the vicinity of the quantum dots. Those defects have a substantial impact on the optical properties of the quantum dots.

1. Introduction

For more than three decades quantum dots (QDs) have attracted significant interest due to their distinct delta-like carrier density of states, relatively strong carrier confinement and unique carrier dynamics [1], which open the possibility for optoelectronic devices with exceptional properties. Self-assembled In(Ga)As QDs grown on GaAs substrates have, after several decades of research, finally fulfilled some of the early predictions for low dimensional semiconductor gain media [2]. Lasers based on QD gain media have the lowest threshold current densities [3] and an insignificant temperature dependence [4], hence providing clear advantages to the more standard quantum well devices [5]. Furthermore, the carrier dynamics in the QD-based gain medium [1,6] have allowed for notably improved temporal and noise performances of lasers [7,8] and optical amplifiers, something that was theoretically predicted prior to the experimental demonstration [9,10]. Unfortunately, In(Ga)As/GaAs QDs on GaAs has a limited spectral coverage of 0.9–1.31 µm. In order to achieve longer wavelength emission, the InP-based material system is mainly used. However, InAs QDs on this substrate have so far not been able to reproduce the outstanding properties of their short wavelength counterparts. Elongated "dash" like QDs [11] or QDs with a high in-plane aspect ratio and a broad size distribution are typically obtained [12]. Although laser devices based on InAs/InP QDs have been demonstrated [13,14], the QD properties need to be significantly improved to achieve desirable device performances. In

#349931 https://doi.org/10.1364/OME.9.001738
Journal © 2019 Received 8 Nov 2018; revised 9 Feb 2019; accepted 12 Feb 2019; published 13 Mar 2019

Optical Materials EXPRESS

particular improvements have to be made on the wetting layer charge leakage, QD size uniformity and shape control [15–17].

A promising alternative approach for the QDs synthesis is selective area growth (SAG) that can potentially address the above-mentioned issues. In comparison to the self-assembled growth technique, where the QD formation process relies on the lattice mismatch between the QD and matrix materials [18,19], in SAG the nucleation occurs in mask openings and is independent on the lattice mismatch. Diblock-copolymer lithography is an advantageous and potentially scalable technique for the fabrication of uniform nanopatterns. Great efforts have been made to understand the principles of thin film polymer self-assembly and to control the properties on demand [20–22]. The diblock-copolymer PS-b-PMMA (polystyrene-b-polymethyl methacrylate), which can form patterns of standing cylinders or spheres with 20 nm feature-sizes, was already applied for SAG of QDs [23,24] and very recently, laser emission was demonstrated from a device based on the gain material of this type [25,26].

In this article, we report on the first realization of selective area droplet epitaxy of an InAs/InP quantum dot array with the assistance of a new diblock-copolymer, PS-b-PDMS (polystyrene-block-polydimethylsiloxane). Detailed optical characterization in the temperature range of 10-300 K allows for the evaluation of the dynamical carrier processes. Due to the significantly greater Flory-Huggins interaction parameter, χ, of PS-b-PDMS, it is possible to form patterns with even smaller characteristic sizes compared to the previously used PS-b-PMMA. Additionally, this copolymer has numerous other advantages, which can significantly simplify the block copolymer lithography process. The developed process allows for the direct deposition of the block copolymer film on a substrate without the need for a brush layer to control the surface energy of the substrate. The specific solvent vapor annealing promotes the self-assembly process and the pattern formation in the film [27,28]. Moreover, PDMS is transforming into a hard mask of silicon oxycarbide while PS cylinders can be etched away by an oxygen plasma [27,29]. Hence, no deposition of an additional dielectric layer and mask transfer is required in the process.

2. Experiment

The fabrication process consisted of two distinct stages: fabrication of a dielectric mask by diblock-copolymer lithography and epitaxial growth of QDs by metal-organic vapor phase epitaxy (MOVPE). Our samples were prepared on 2" n-type InP substrates with (001)-orientation. All the epitaxial processes were carried out using a low-pressure (60 Torr) Turbodisc MOVPE system with trimethylindium (TMIn), arsine (AsH_3) and phosphine (PH_3) as precursors, and hydrogen (H_2) as carrier gas. As a first step, we epitaxially deposited 450 nm of undoped InP.

Mask fabrication: The mask fabrication process is schematically illustrated in Fig. 1(a-c). PS-b-PDMS powder (61–111 K) was dissolved in cyclohexane 1/400 mg/ml and spin-casted onto the wafer forming an ultrathin film of 28–30 nm (Fig. 1(a)). Ellipsometry measurements verified the film thickness. To stimulate the polymer pattern formation, the sample was placed in a chamber with methylcyclohexane saturated vapor until the pattern of standing cylinders was formed (Fig. 1(b)). Scanning electron microscopy (SEM) was afterwards used to investigate the resulting pattern.

To transform PS-b-PDMS patterned films into a hard mask, an inductively coupled plasma-reactive ion etching (ICP-RIE) process was carried out. A short sulfur hexafluoride plasma etch of 10 s was applied in the beginning to remove the thin PDMS skin layer on top of the polymer film and to open the PS cylinders [27]. The following 26 s oxygen plasma etch removed the PS cylinders and oxidized the PDMS matrix. As a result, the PS-b-PDMS patterned film was transformed into a silicon oxycarbide hard mask with openings of ~30 nm in diameter and ~75 nm pitch (Fig. 1(c)). The masks were afterwards inspected with a SEM and an atomic force microscope (AFM).

Optical Materials EXPRESS

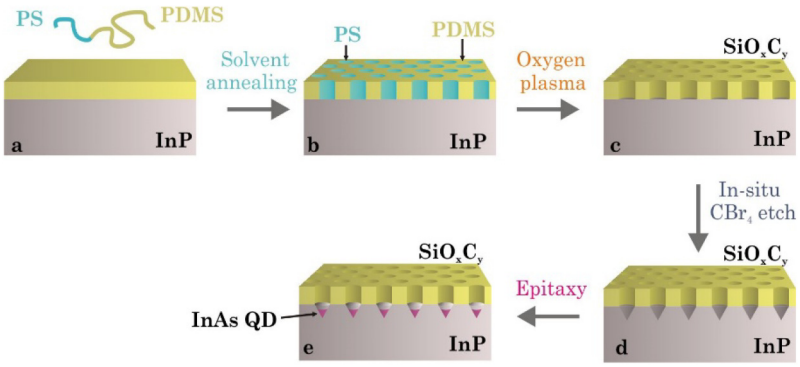

Fig. 1. Schematic illustration of the mask fabrication and QD growth process.

Selective area epitaxy: Prior to the selective epitaxial growth step, the wafer with the mask on top was cleaned by dipping it into concentrated sulfuric acid for 2 min followed by 3 min rinsing in de-ionized water with nitrogen bubbles. After drying with nitrogen gas, the wafer was loaded into the MOVPE chamber. Then, an annealing step was carried out under phosphine ambient at 550 – 650 °C for 15 min. The next step was in-situ InP etching by carbon tetrabromide (CBr_4) in the mask openings to form an array of holes (Fig. 1(d)). Prior to the QD deposition, the temperature was lowered to 450 °C and the sample was exposed to AsH_3 for 27 s. Indium droplets were deposited in the etched holes for 3 s with TMIn flow of 0.23 µmol/min in the absence of any V^{th} group precursor in the growth chamber. Annealing the indium droplets in AsH_3 ambient for 60 s promotes their crystallization into InAs following the structure of the InP crystal lattice. InAs QDs were capped first by 3 nm, and next by 5 nm of InP deposited at 450 °C and 550 °C, respectively (Fig. 1(e)). After this, a short annealing at 550 °C in PH_3 ambient was done to promote out diffusion of point defects formed because of the low growth temperature [30].

Optical characterization. For the spectroscopic experiments, the structure with SAG InAs/InP QDs was held in a variable-temperature optical cryostat allowing for control of the sample temperature in the range between 10 and 300 K. For time-integrated and time-resolved photoluminescence (PL) experiments, the sample was excited by a train of ~160 fs long pulses with ~13.2ns pulse-to-pulse distance. The pulse train either came from a mode-locked Ti:Sapphire laser (Coherent Mira-HP) operating at the wavelength of 832 nm (~1.48 eV), or a synchronously pumped optical parametric oscillator (Coherent/APE OPO-HP), providing pulses with a wavelength of 1.4 μm (~0.89 eV). Emission from the structure was collected in a standard far-field optical setup and dispersed by a monochromator with a focal length of 0.3 m (Princeton Instruments Acton SP2300i). The time-integrated PL spectra were measured via the lock-in technique (Signal Recovery 7560) at a carrier frequency of 2 kHz, using a liquid-nitrogen-cooled InSb photoconductive single channel detector (Hamamatsu P7751-02). Time-resolved photoluminescence (TRPL) was measured with a near-infrared streak camera system (Hamamatsu C112930-02) operating in the single-photon counting regime with a minimum time-resolution of ~20 ps.

3. Results and discussion

3.1. Fabrication

Block-copolymer lithography. The surface energy of the wafer has a large influence on the process of polymer self-assembly. Water drop contact angle measurements were used to quantify the difference in surface energy between epitaxially grown InP and standard Si wafers on which the lithography process was originally developed. By these measurements, we recognized that the

Optical Materials EXPRESS

oxygen plasma treatment allowed changing the surface energy of InP to be close to the one of Si. The contact angle on the untreated epitaxial InP is 67 ± 12° whereas immediately after exposure to the oxygen plasma it changes to 26 ± 5°. The contact angle on Si is 18 ± 3°. By applying this method the desired pattern of standing PS cylinders of about 30 nm in diameter was achieved after annealing the PS-b-PDMS film with a thickness of 28–30 nm in methylcyclohexane saturated vapor for 55 min at 21 °C. The presence of short-range hexagonal order indicates a standing cylinder pattern, while the absence of such order is typical for the spherical polymer phase [31]. The self-assembly process of block-copolymer is susceptible to the annealing time. Already a 5-minute deviation induces significant defects of a different polymer phase. Temperature and humidity also influence the self-assembly process, and the film thickness should obey the commensurability condition. A deviation in film thickness leads to terracing, which results in a nonuniform pattern phase [32].

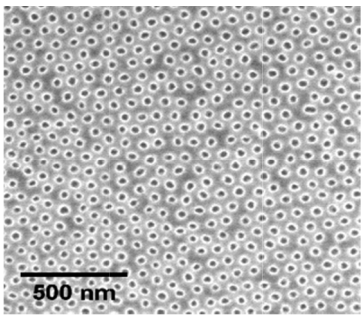

Fig. 2. SEM image of SiO_xC_y hard mask.

After the pattern formation a top PDMS layer covers the pattern [33] and therefore it is essential to remove this layer by a short sulfur hexafluoride plasma etch before the oxygen plasma step. Otherwise the top layer will be oxidized and will not allow for etching of PS cylinders. We hence investigated the mask with a SEM (Fig. 2) and an AFM equipped with an ultrathin Bruker ScanAsyst-AIR tip to make sure that the mask openings are completely revealed.

Growth of quantum dots. Prior to the epitaxial growth the wafer is exposed to a high-temperature annealing step in phosphine overpressure to remove the native oxide from the semiconductor surface. However, annealing InP wafers covered by the SiO_xC_y mask at the standard temperature of 650 °C in phosphine ambient resulted in the formation of InP surface defects while the mask in those areas was membranized. A representative SEM image showing such defects is presented in Fig. 3(a). By lowering the annealing temperature down to 550 °C the formation of those under-etch defects was avoided. A similar problem was described in [25], which in this case was attributed to CBr_4 under-etching, while in our case the high temperature is responsible for InP etching. During the annealing step, not only the native oxide but also InP in the mask openings is desorbed, and those thermo-etched areas from neighboring openings merge forming surface defects. Since the etch rate is different for different crystallographic planes, the etched pits have faceting by opening {111} family planes. Those defects are clearly seen on the SEM image presented in Fig. 3(b) taken after the mask removal. Lower annealing temperatures can result in incomplete de-oxidation, but an increase in annealing time can compensate for this. The efficiency of de-oxidation was indirectly evaluated by measuring PL from the QD array.

We employ CBr_4 for in-situ etching in the MOVPE chamber inside the mask openings. There are two purposes for this. The first purpose is to remove areas with a high density of point crystal defects after plasma etching and to improve the interface quality [34]. These point defects could act as nonradiative recombination centers. The second purpose is to etch holes in InP to bury QDs in those holes and to control their shape. The etch process is self-limited and strongly

Optical Materials EXPRESS

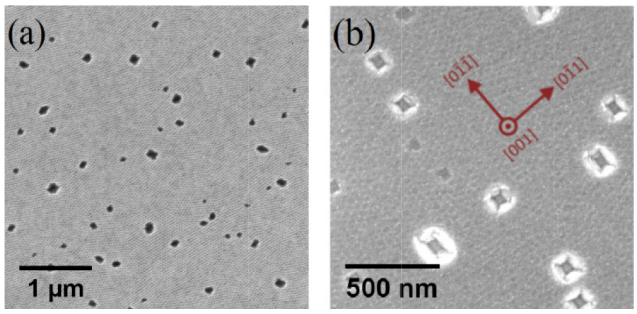

Fig. 3. (a) InP surface defects formed underneath the SiO_xC_y mask after 650 °C annealing. (b) The same sample after the mask is removed. The red arrows indicate the crystallographic orientations.

depends on the crystallographic orientation, dominantly opening the {111} family planes [35]. The etching time of 20 s was kept short to avoid possible etching of InP under the mask and merging of etched pits [25].

3.2. Optical characterization

Time-integrated photoluminescence studies. A series of PL spectra obtained in the temperature range of 10-300 K for the investigated structure is presented in Fig. 4(a). The spectra are

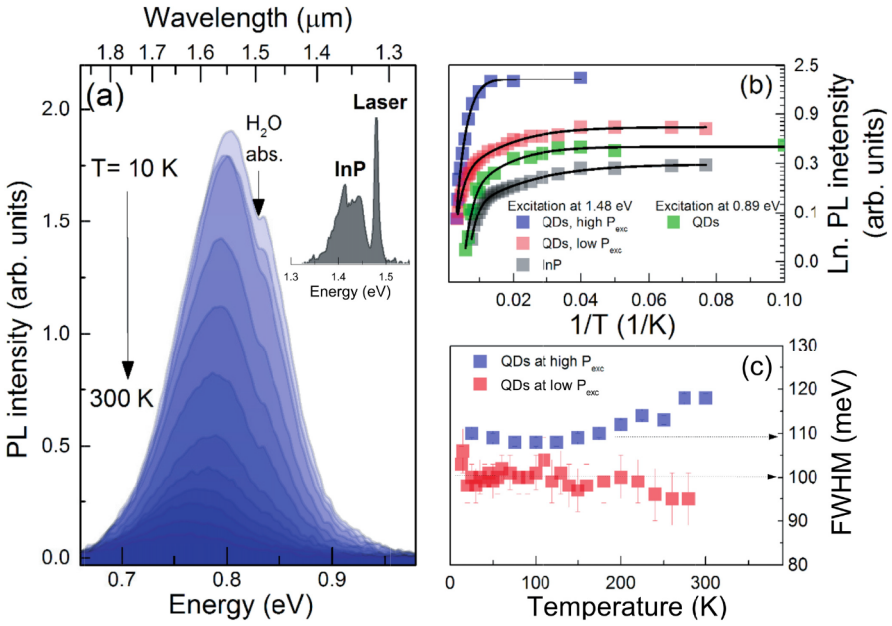

Fig. 4. (a) Temperature dependence of PL emission from SAG InAs/InP QDs (E_{exc} = 1.48 eV, $P_{exc} \approx 5.5$ W/cm^{-2}). Inset: PL emission from the InP barrier and the laser spectrum at T = 10 K. (b) Temperature PL quenching for QDs measured under high/low excitation power above InP barrier (red and blue squares) and below InP barrier excitation under low excitation power (green squares), and the PL quench for InP barrier under low excitation power (black squares). These dependences are arbitrary shifted on the intensity scale for better visibility. (c) The Full-Width-at-Half-Maximum (FWHM) parameter for the QDs PL band for two optical pumping powers.

Optical Materials EXPRESS

measured under conditions of above InP barrier excitation and with a relatively high optical pumping power density ($P_{exc} \approx 5.5$ W/cm^{-2}). The PL spectrum from SAG InAs/InP QDs is centered at ~0.8 eV (~0.76 eV) at T = 10 K (300 K) and covers the C- and L- telecom spectral windows. Each PL band was fitted to a Gaussian profile allowing for the extraction of the peak intensity (Fig. 4(b)) and its full width at half maximum - FWHM (Fig. 4(c)) in order to evaluate the carrier confinement in the dots.

Since the band offset of the strained InAs/InP material system is expected to be ~300 meV for the conduction band, and ~500 meV for the valence band [36], the carrier confinement in InAs/InP QDs should be rather strong. It is relevant to investigate the temperature impact on the carrier distribution among QD ground states (GSs) and the efficiency of the QD emission process. The PL intensity for the SAG QDs plotted as a function of inverse temperature, T, is shown in Fig. 4(b). We investigated different excitation regimes. (i) The excitation energy tuned above the InP barrier, $E_{exc} = 1.48$ eV, and high excitation power density $P_{exc} \approx 5.5$ W/cm^2 (blue squares), (ii) $E_{exc} = 1.48$ eV, and low $P_{exc} \approx 0.6$ W/cm^2 (red squares), and (iii) quasi-resonant excitation of the dots, $E_{exc} = 0.89$ eV, nearly 0.53 eV below the InP bandgap and low $P_{exc} \approx 0.6$ W/cm^2 (green squares). In addition, the PL thermal quench for InP is presented in Fig. 4(b) (black squares), obtained under $E_{exc} = 1.48$ eV, and $P_{exc} \approx 0.6$ W/cm^2. The PL quenches in Fig. 4(b) are arbitrarily shifted on the intensity scale for easier mutual comparison. Each experimental trend is fitted (solid black lines) by a widely used steady-state solution for the thermal rate equation expressed as:

$$I(T) = I_0 \Big/ \left(1 + \sum_{i=1}^{n} C_i e^{-E_{a,i}/k_B T}\right), \quad (1)$$

where C_i is the pre-exponential factor for the i^{th} thermal activation process [37], $E_{a,i}$ is the activation energy related to the i^{th} process, k_B is the Boltzmann constant, T is the temperature and I_0 is the extrapolated PL signal intensity at 0 K. In all the cases, experimental data points and fitting curves well converged when two thermal activation processes are considered (i = 1,2) in Eq. (1). The resulting best fitting parameters are summarized in Table 1.

Table 1. Parameters of the PL thermal quenching.

PL emission	$E_{a,1}$, (meV)	$E_{a,2}$, (meV)	C_1	C_2	Excitation, (eV)	Pumping power
QDs	38 ± 9	109 ± 50	25	582	Above InP (1.48 eV)	High
QDs	56 ± 10	7 ± 3	34	2	Above InP (1.48 eV)	Low
InP	54 ± 10	6 ± 1	34	2	Above InP (1.48 eV)	Low
QDs	61 ± 23	9 ± 3	23	3	Quasi-resonantly in QDs (0.89 eV)	Low

While the pre-exponential factors C_i cannot be easily compared due to the different excitation regimes, one can compare the activation energies. For the PL thermal quench measured for SAG QDs under high and low P_{exc} and $E_{exc} = 1.48$ eV, both $E_{a,1}$ activation energies can be considered as similar owing to the same activation mechanism that dominates the PL quench independently on the optical power density. In contrast, the $E_{a,2}$ energies are much different, indicating different activation processes. Their visibility in the overall PL quench depends on the occupation factor of the density of states (DOS) in the structure and the temperature range. On one side, the process with a higher activation energy $E_{a,2} = 109 \pm 50$ meV can be tracked only under high photo-excitation and at T > 200 K. On the other side, the process with the low activation energy $E_{a,2} = 7 \pm 3$ meV is already present in the low-temperature regime 15 K < T < 100 K. Most likely, its visibility depends on the occupation factor of the DOS addressed during the photo-excitation. Intriguing is to compare the PL quench parameters for the InP barrier and SAG QDs, since they are very similar within the uncertainty of the fitting parameters. This observation suggests that the recorded PL quench of SAG QD emission is controlled by thermal processes occurring in

Optical Materials EXPRESS

the barrier DOS. This conclusion is further strengthened by comparison to the PL quench for QDs excited quasi-resonantly. The respective activation energies are the same as those obtained for above-barrier excitation (see Table 1). Therefore, the PL quench observed for SAG QDs cannot be discussed in terms of common thermal activation mechanisms like carrier re-excitation from the QD GS to higher-lying energy states within the confinement potential of a dot or to the wetting layer. To describe the observed behavior, we suggest the following scenario: a population of photo-generated carriers is effectively trapped by an extensive DOS located within the InP bandgap, and subsequently, it is only partially transferred to QDs. With the increase of temperature, a certain population of trapped carriers is released from their localized potentials in the barrier with the localization depth of roughly 7 and 60 meV (Table 1). Thermally activated carriers, in their vast majority, are non-radiatively lost in the barrier and the efficiency of these processes increases with T. It causes that less and less carriers feed the QD states with increasing T. The nature of carrier localized states in the InP bandgap is related to various lithography steps like impurity levels and defect states at the native oxide/InP interface as well as structural defects formed in the InP matrix during ICP dry etching. Under the incomplete de-oxidation of InP, one can point to In_P^{-1} [38] and O_P^0 that create trap states near the conduction band edge, where the former is localized ~60 meV below the conduction band edge of InP and the latter is located deep inside the InP bandgap, as suggested in [39]. The In_P^{-1} defect level can be responsible for the observation of the ~60 meV activation energy causing the temperature-induced PL quench.

The investigation of the temperature-induced quench of SAG QD PL emission indicates that the barrier DOS has a significant impact on the optical characteristics of these dots and influences the carrier redistribution process among the QD ensemble. Fig. 4(c) presents the FWHM of the peak emission of SAG QDs. At low temperatures, the FWHM largely reflects substantial dot-to-dot inhomogeneity in size, shape, and chemical content across their ensemble. In the temperature range of 10-300 K, the FWHM changes only slightly within 5% of the value. From 10 K up to ~200 K the changes are even smaller, and the FWHM is considered to be constant for a given P_{exc}. Carrier redistribution processes among dots can be deduced from the PL quench characteristics at T > 200 K and high P_{exc}. For $P_{exc} \approx 0.6$ W/cm^2, the FWHM decreases with T, while for $P_{exc} \approx 5.5$ W/cm^2 it increases. The decrease can be interpreted as a speedup of the carrier losses in the barrier owing to population of a smaller ensemble of QD states having a more profound confining potential. The increase can be related to the population of a broader ensemble of QDs and their excited states, both in the vicinity of carrier migration in the barrier DOS. Despite that, the observed small changes in the FWHM at low and room temperatures suggest in average strong carrier confinement in the dots weakly affected by the thermal environment.

Time-resolved photoluminescence studies. The results of the time-resolved (TR) PL experiments are summarized in Fig. 5. The excitation is provided at $E_{exc} = 1.48$ eV, and $P_{exc} \approx 0.6$ W/cm^2. The examples of intensity-normalized TRPL traces obtained at the center-of-mass of the PL emission from SAG QDs are presented in Fig. 5(a). Similar TRPL traces have been measured for different emission energies around the PL peak energy to evaluate the possible effect of carrier redistribution among QDs.

Each TRPL trace is characterized by a substantial delay after the photo-excitation during which the PL signal reaches its maximum amplitude, Fig. 5(b). The numerical fit to the experimental data, assuming a bi-exponential decay and single exponential rise, results in two decay time parameters, $\tau_{PLdec,1}$ and $\tau_{PLdec,2}$, and the rise time parameter, τ_{rise}, summarized in Fig. 5(c), and (d), respectively, plotted as a function of temperature and the emission energy.

At T = 10 K, when the phonon population is negligible, one can assume that the PL dynamics are mostly determined by the confining potential of a QD. In this case, a TRPL trace is characterized by the PL rise time of ~200 ps, and a single PL decay time of ~1 ns. The second PL decay component cannot be resolved in this case due to its small amplitude. The PL rise time can be related to the sum of capture and the intra-band carrier relaxation times in the dot, after which

Optical Materials EXPRESS

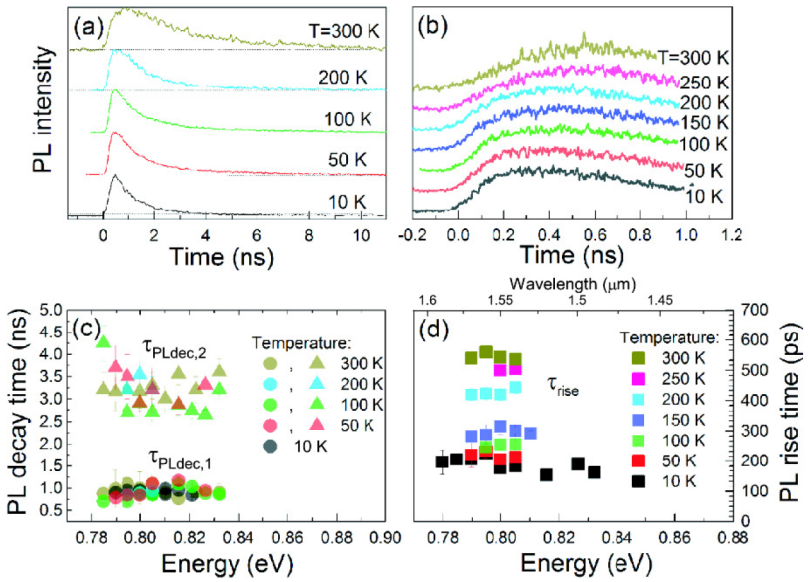

Fig. 5. (a) Time-resolved photoluminescence (TRPL) traces for selective-area growth InAs/InP QDs at various temperatures. (b) TRPL traces at their initial time-period after photo-excitation. (c) Dispersion of photoluminescence decay times at various temperatures, (d) dispersion of photoluminescence rise times as a function of temperature.

the occupation of QD states reaches its quasi-equilibrium. Such an elongated τ_{rise} is rather unusual for QDs. For a self-assembled InAs/GaAs QD the intra-band relaxation time reaches several ps [40]. In a very recent study on intra-band carrier relaxation times in self-assembled InAs/InP QDs it was shown that relaxation time can be as short as 8 ps at cryogenic temperatures, even including the capture time [41]. For a comparable QD system like InAs/InAlAs/InP(001) [42] and InAs/InP(311B) [43], or InAs/InGaAsP/InP(001) quantum dashes [44], the intra-band relaxation time is reported to be within the range of 1-40 ps. However, in the SAG QDs, τ_{rise} can be dominated by the capture time, which further will be discussed by the temperature-induced trend presented in Fig. 5 (d). The PL decay is a more puzzling issue. On the one hand, theoretical studies on an electron-hole (e-h) pair strongly confined in an InAs/InP QD have predicted the e-h radiative lifetime in the range of 1.6-2.4 ns depending on the dot size [45]. On the other hand, for large and strongly elongated InAs/InAlGaAs/InP QDs, where the e-h pair is in the intermediate confinement regime, the e-h can radiate into two superimposed lifetime components of ~1 ns and ~2 ns [46]. Although the latter would match with the obtained experimental results on SAG QDs, especially at higher temperatures, the estimated small size of the dots pushes the interpretation towards the e-h pair lifetime resulting from the strong confinement regime. However, one has to be aware that the PL lifetime can be slightly modified by the coupling of QD confined states to the surface states through the ~8 nm thick InP barrier above the dot. While a hole is more likely localized in the dot due to its effective mass, an electron wavefunction can penetrate through the barrier to surface DOS decreasing the e-h overlap in the dot and thus increasing the PL lifetime.

In Fig. 5(c) and (d) we present temperature induced changes in the PL rise and decay times. One can observe that both components of the PL decay are barely changed with T, while the $\tau_{\text{PLdec,1}} \approx 1$ ns, the $\tau_{\text{PLdec,2}}$ is spread between 2.7 and 4.2 ns without any general trend. The spread is mostly generated by the accuracy of the fitting procedure and can also be attributed to the coupling of QD states to the surface DOS. In general, each of the PL decay components is contributed by radiative (τ_{rad}) and non-radiative ($\tau_{\text{non-rad}}$) recombination processes,

Optical Materials EXPRESS

$\tau_{PLdec}{}^{-1}=\tau_{rad}{}^{-1}+\tau_{non-rad}{}^{-1}(T)$. While the already discussed τ_{rad} is temperature independent for a QD, the $\tau_{non-rad}$ can strongly depend on T. Increasing the phonon population number with T leads to more efficient carrier-phonon scattering processes and thus shorter $\tau_{non-rad}$, resulting in a shorter τ_{PLdec}. This typically leads to the observation of the time-integrated temperature-induced PL quench in self-assembled QDs, which is not the case for the studied SAG QDs where non-radiative recombination occurs predominantly in the barrier DOS. A similar effect has been observed for self-assembled InAs/GaAs QDs [47]. Moreover, the lack of strong temperature dependence of the PL lifetime suggests that the above mentioned coupling of QD states to surface states is weak, the e-h correlation remains stabilized by the QD confinement, and surface states weakly participate in the non-radiative losses to quantum dots.

Another interesting point is the lack of any spectral dispersion for the obtained $\tau_{PLdec,1}(T)$, $\tau_{PLdec,2}(T)$, and $\tau_{rise}(T)$ functions presented in Fig. 5 (c) and (d). Along with the lack of a significant change in the FWHM parameter presented in Fig. 4 (c), this observation suggests negligible carrier migration between QDs and thus a relatively strong e-h confinement in the dot modified by the presence of the barrier DOS.

Finally, for the SAG QDs, the τ_{rise} depends strongly on T, as presented in Fig. 5(d). With increasing T from 10 K to 300 K, the τ_{rise} increases from ~200 ps to ~560 ps. We previously argued that τ_{rise} is mainly dominated by the carrier capture time from the barrier to QDs. Additionally, we presented evidence for the existence of an extended DOS in the barrier that accumulates a significant portion of carriers after their photo-generation. These arguments lead to the conclusion that the elongated τ_{rise} is most likely related to charge migration within the barrier DOS before they are captured by QDs. A similar effect has been shown for self-assembled (In,Ga)As/GaAs QDs placed on a wetting layer with a sizable zero-dimensional density of states in there [48]. If the spatially distributed DOS outside the QDs is larger than the dot density, then the carrier capture time can be controlled by a time-consuming temperature-induced hopping process among spatially distributed states in the barrier.

4. Conclusion

In conclusion, we present selective area growth of InAs/InP quantum dots assisted by block-copolymer lithography. We developed the fabrication method of silicon oxycarbide hard masks with cylindrical openings of 30 nm in diameter on top of an InP substrate. The pattern parameters could be regulated by manipulating the self-assembly process in PS-b-PDMS block-copolymer. We carried out a systematic investigation of the carrier dynamics in an array of SAG QDs using time-integrated PL and temperature dependent TRPL measurements. The SAG QDs demonstrate strong carrier localization, however, their emission properties are affected by the defect-related density of states located in the InP barrier in the close vicinity of the dots. It is found that these states act as a carrier reservoir for the dots and dominate temperature-induced carrier migration in the structure. The effect is seen despite of a strong PL quench from QDs accompanied by negligible changes in the PL decay time in the whole temperature range between 10 and 300 K. This explanation is further supported by a slow and elongated temperature carrier capture time by the dots ranging from 200–500 ps. The nature of those defects is likely related to the technological process, the contamination with foreign atoms introduced during the lithography steps and damage of the crystal lattice during the ICP dry etching process.

Funding

Villum Fonden via the NATEC Centre (8692); YIP QUEENs (VKR023442); Ministerstwo Nauki i Szkolnictwa Wyższego (DI 2017 011747); Danish National Research Foundation (DNRF103).

Optical Materials EXPRESS

Acknowledgements

The authors thank Alexander Huck for fruitful discussions.

References

1. A. Markus, J. X. Chen, C. Paranthoën, A. Fiore, C. Platz, and O. Gauthier-Lafaye, "Simultaneous two-state lasing in quantum-dot lasers," Appl. Phys. Lett. **82**(12), 1818–1820 (2003).
2. Y. Arakawa and H. Sakaki, "Multidimensional quantum well laser and temperature dependence of its threshold current," Appl. Phys. Lett. **40**(11), 939–941 (1982).
3. G. Park, O. B. Shchekin, D. L. Huffaker, and D. G. Deppe, "Low-threshold oxide-confined 1.3-μm quantum-dot laser," IEEE Photonics Technol. Lett. **12**(3), 230–232 (2000).
4. O. B. Shchekin, J. Ahn, and D. G. Deppe, "High temperature performance of self-organised quantum dot laser with stacked p-doped active region," Electron. Lett. **38**(14), 712 (2002).
5. A. E. Zhukov, A. R. Kovsh, S. S. Mikhrin, A. P. Vasil'ev, E. S. Semenova, N. A. Maleev, V. M. Ustinov, M. M. Kulagina, E. V. Nikitina, I. P. Soshnikov, Y. M. Shernyakov, D. A. Livshits, N. V. Kryjanovskaya, D. S. Sizov, M. V. Maximov, A. F. Tsatsul'nikov, N. N. Ledentsov, D. Bimberg, and Z. I. Alferov, "High external differential efficiency and high optical gain of long-wavelength quantum dot diode laser," Phys. E **17**, 589–592 (2003).
6. T. Akiyama, M. Sugawara, and Y. Arakawa, "Quantum-Dot Semiconductor Optical Amplifiers," Proc. IEEE **95**(9), 1757–1766 (2007).
7. K. Yvind, D. Larsson, J. Mørk, J. M. Hvam, M. Thompson, R. Penty, and I. White, "Low-noise monolithic mode-locked semiconductor lasers through low-dimensional structures," in A. A. Belyanin and P. M. Smowton, eds. (2008), p. 69090A.
8. A. Kovsh, A. Gubenko, I. Krestnikov, D. Livshits, S. Mikhrin, J. Weimert, L. West, G. Wojcik, D. Yin, C. Bornholdt, N. Grote, M. V. Maximov, and A. Zhukov, "Quantum dot comb-laser as efficient light source for silicon photonics," in G. C. Righini, S. K. Honkanen, L. Pavesi, and L. Vivien, eds. (International Society for Optics and Photonics, 2008), Vol. 6996, p. 69960 V.
9. T. W. Berg and J. Mørk, "Theoretical analysis of quantum dot amplifiers with high saturation power and low noise figure," in *ECOC 2002 Proceedings* (IEEE, 2002), Vol. 2, pp. 1–2.
10. T. W. Berg and J. Mørk, "Quantum dot amplifiers with high output power and low noise," Appl. Phys. Lett. **82**(18), 3083–3085 (2003).
11. R. Wang, A. Stintz, and P. Varangis, "Room-temperature operation of InAs quantum-dash lasers on InP," IEEE Photonics Technol. Lett. **13**(8), 767–769 (2001).
12. E. S. Semenova, I. V. Kulkova, S. Kadkhodazadeh, M. Schubert, R. E. Dunin-Borkowski, and K. Yvind, "InAs/InGaAsP Quantum Dots Emitting at 1.5 μm for Applications in Lasers," *Conf. Proc. - Int. Conf. Indium Phosphide Relat. Mater. IEEE* (2011).
13. Y. Yu, W. Xue, E. Semenova, K. Yvind, and J. Mork, "Demonstration of a self-pulsing photonic crystal Fano laser," Nat. Photonics **11**(2), 81–84 (2017).
14. W. Xue, Y. Yu, L. Ottaviano, Y. Chen, E. Semenova, K. Yvind, and J. Mork, "Threshold Characteristics of Slow-Light Photonic Crystal Lasers," Phys. Rev. Lett. **116**(6), 063901 (2016).
15. D. Miller, "Device Requirements for Optical Interconnects to Silicon Chips," Proc. IEEE **97**(7), 1166–1185 (2009).
16. B. Ellis, M. A. Mayer, G. Shambat, T. Sarmiento, J. Harris, E. E. Haller, and J. Vučković, "Ultralow-threshold electrically pumped quantum-dot photonic-crystal nanocavity laser," Nat. Photonics **5**(5), 297–300 (2011).
17. M. T. Hill and M. C. Gather, "Advances in small lasers," Nat. Photonics **8**(12), 908–918 (2014).
18. Y. D. Galeuchet, R. Hugo, and P. Roentgen, "MOVPE on patterned substrates: a new fabrication method for nanometer structure devices," Microelectron. Eng. **15**(1-4), 667–670 (1991).
19. T. Fukui, S. Ando, Y. Tokura, and T. Toriyama, "GaAs tetrahedral quantum dot structures fabricated using selective area metalorganic chemical vapor deposition," Appl. Phys. Lett. **58**(18), 2018–2020 (1991).
20. R. A. Segalman, "Patterning with block copolymer thin films," Mater. Sci. Eng., R **48**(6), 191–226 (2005).
21. H. Yoshida and M. Takenaka, "Physics of block copolymers from bulk to thin films," in *Directed Self-Assembly of Block Co-Polymers for Nano-Manufacturing* (Elsevier, 2015), pp. 3–26.
22. I. W. Hamley, "Ordering in thin films of block copolymers: Fundamentals to potential applications," Prog. Polym. Sci. **34**(11), 1161–1210 (2009).
23. J. H. Park, C.-C. Liu, M. K. Rathi, L. J. Mawst, P. F. Nealey, and T. F. Kuech, "Nanoscale selective growth and optical characteristics of quantum dots on III-V substrates prepared by diblock copolymer nanopatterning," J. Nanophotonics **3**(1), 031604 (2009).
24. E. S. Semenova, I. V. Kulkova, S. Kadkhodazadeh, D. Barettin, O. Kopylov, A. Cagliani, K. Almdal, M. Willatzen, and K. Yvind, "Epitaxial growth of quantum dots on InP for device applications operating at the 1.55 μm wavelength range," Proc. SPIE **8996**, 899606 (2014).
25. H. Kim, J. Choi, Z. Lingley, M. Brodie, Y. Sin, T. F. Kuech, P. Gopalan, and L. J. Mawst, "Selective growth of strained (In)GaAs quantum dots on GaAs substrates employing diblock copolymer lithography nanopatterning," J. Cryst. Growth **465**, 48–54 (2017).

Optical Materials EXPRESS

26. H. Kim, W. Wei, T. F. Kuech, P. Gopalan, and L. J. Mawst, "Quantum Dot Laser Diodes emitting 1 . 57 ~ 1 . 67μm at room temperature grown by Block Copolymer Lithography and Selective Area MOCVD," *2018 IEEE Int. Semicond. Laser Conf.* 63–64 (2018).
27. Y. S. Jung and C. A. Ross, "Solvent-Vapor-Induced Tunability of Self-Assembled Block Copolymer Patterns," Adv. Mater. **21**(24), 2540–2545 (2009).
28. K. W. Gotrik, A. F. Hannon, J. G. Son, B. Keller, A. Alexander-Katz, and C. A. Ross, "Morphology Control in Block Copolymer Films Using Mixed Solvent Vapors," ACS Nano **6**(9), 8052–8059 (2012).
29. T. Li, Z. Wang, L. Schulte, and S. Ndoni, "Substrate tolerant direct block copolymer nanolithography," Nanoscale **8**(1), 136–140 (2016).
30. C. Dion, P. Desjardins, N. Shtinkov, F. Schiettekatte, P. J. Poole, and S. Raymond, "Effects of grown-in defects on interdiffusion dynamics in InAs/InP(001) quantum dots subjected to rapid thermal annealing," J. Appl. Phys. **103**(8), 083526 (2008).
31. T. Li, Z. Wang, L. Schulte, O. Hansen, and S. Ndoni, "Fast & scalable pattern transfer via block copolymer nanolithography," RSC Adv. **5**(124), 102619 (2015).
32. A. P. Smith, J. F. Douglas, J. C. Meredith, E. J. Amis, and A. Karim, "Combinatorial Study of Surface Pattern Formation in Thin Block Copolymer Films," Phys. Rev. Lett. **87**(1), 015503 (2001).
33. T. Li, "Functional materials derived from block copolymer self-assembly," PhD thesis, DTU Nanotech (2015).
34. S. Arakawa, M. Ito, R. Nakasaki, and A. Kasukawa, "Improvement of MOCVD Growth Technique Using CBr4," *Furukawa Rev.* 76–81 (2003).
35. N. Kuznetsova, I. V. Kulkova, E. S. Semenova, S. Kadhodazadeh, N. V. Kryzhanovskaya, A. E. Zhukov, and K. Yvind, "Crystallographic dependent in-situ CBr4 selective nano-area etching and local regrowth of InP/InGaAs by MOVPE," J. Cryst. Growth **406**, 111–115 (2014).
36. M. Gong, K. Duan, C.-F. Li, R. Magri, G. A. Narvaez, and L. He, "Electronic structure of self-assembled In As/InP quantum dots: Comparison with self-assembled In As/GaAs quantum dots," Phys. Rev. B **77**(4), 045326 (2008).
37. M. A. Reshchikov, "Temperature dependence of defect-related photoluminescence in III-V and II-VI semiconductors," J. Appl. Phys. **115**(1), 012010 (2014).
38. R. Mishra, O. D. Restrepo, A. Kumar, and W. Windl, "Native point defects in binary InP semiconductors," J. Mater. Sci. **47**(21), 7482–7497 (2012).
39. D. Ko, X. W. Zhao, K. M. Reddy, O. D. Restrepo, R. Mishra, T. R. Lemberger, I. S. Beloborodov, N. Trivedi, N. P. Padture, W. Windl, F. Y. Yang, and E. Johnston-Halperin, "Defect states and disorder in charge transport in semiconductor nanowires," J. Appl. Phys. **114**(4), 043711 (2013).
40. H. Kurtze, J. Seebeck, P. Gartner, D. R. Yakovlev, D. Reuter, A. D. Wieck, M. Bayer, and F. Jahnke, "Carrier relaxation dynamics in self-assembled semiconductor quantum dots," Phys. Rev. B **80**(23), 235319 (2009).
41. M. Syperek, J. Andrzejewski, E. Rogowicz, J. Misiewicz, S. Bauer, V. I. Sichkovskyi, J. P. Reithmaier, and G. Sęk, "Carrier relaxation bottleneck in type-II InAs/InGaAlAs/InP(001) coupled quantum dots-quantum well structure emitting at 1.55 μ m," Appl. Phys. Lett. **112**(22), 221901 (2018).
42. E. Péronne, F. Fossard, F. H. Julien, J. Brault, M. Gendry, B. Salem, G. Bremond, and A. Alexandrou, "Dynamic saturation of an intersublevel transition in self-organized InAs/InxAl1 − x As quantum dots," Phys. Rev. B **67**(20), 205329 (2003).
43. P. Miska, J. Even, O. Dehaese, and X. Marie, "Carrier relaxation dynamics in InAs/InP quantum dots," Appl. Phys. Lett. **92**(19), 191103 (2008).
44. M. Syperek, Ł. Dusanowski, J. Andrzejewski, W. Rudno-Rudziński, G. Sęk, J. Misiewicz, and F. Lelarge, "Carrier relaxation dynamics in InAs/GaInAsP/InP(001) quantum dashes emitting near 1.55 μm," Appl. Phys. Lett. **103**(8), 083104 (2013).
45. M. Gong, W. Zhang, G. Can Guo, and L. He, "Atomistic pseudopotential theory of optical properties of exciton complexes in InAs/InP quantum dots," Appl. Phys. Lett. **99**(23), 231106 (2011).
46. M. Gawełczyk, M. Syperek, A. Maryński, P. Mrowiński, Ł. Dusanowski, K. Gawarecki, J. Misiewicz, A. Somers, J. P. Reithmaier, S. Höfling, and G. Sęk, "Exciton lifetime and emission polarization dispersion in strongly in-plane asymmetric nanostructures," Phys. Rev. B **96**(24), 245425 (2017).
47. K. Mukai, N. Ohtsuka, and M. Sugawara, "High photoluminescence efficiency of InGaAs/GaAs quantum dots self-formed by atomic layer epitaxy technique," Appl. Phys. Lett. **70**(18), 2416–2418 (1997).
48. M. Syperek, M. Baranowski, G. Sęk, J. Misiewicz, A. Löffler, S. Höfling, S. Reitzenstein, M. Kamp, and A. Forchel, "Impact of wetting-layer density of states on the carrier relaxation process in low indium content self-assembled (In,Ga)As/GaAs quantum dots," Phys. Rev. B **87**(12), 125305 (2013).